Controlling Density Fluctuations in Wall-Bounded Dissipative Particle Dynamics Systems

Igor V. Pivkin* and George Em Karniadakis†

Division of Applied Mathematics, Brown University, Providence, Rhode Island 02912, USA

(Received 7 October 2005; published 26 May 2006)

Dissipative Particle Dynamics (DPD) simulations of wall-bounded flows exhibit density fluctuations that depend strongly on the no-slip boundary condition and increase with the level of coarse graining. We develop an adaptive model for wall-particle interactions that eliminates such oscillations and can target prescribed density profiles. Comparisons are made with ideal no-slip boundary conditions and molecular dynamics simulations. The new model is general and can be used in other coarse-grained particle methods.

DOI: 10.1103/PhysRevLett.96.206001 PACS numbers: 83.10.Pp, 83.10.Rs, 82.70.Dd

Interaction of liquids with solid walls causes layering of the fluid atoms, which is responsible for the large density fluctuations very near the wall [1]. Targeting specific density profiles is an important problem in microfluidic mixing, interfacial phenomena, and other nanotechnology applications. For example, water density profiles play an important role in regulating ion and macromolecule transport, e.g., ion-water and water-macromolecule interactions play a central role. The water-ion and water-DNA interactions can be regulated by controlling the water density profiles. Molecular dynamics (MD) simulations with properly formulated interaction potentials have provided great insight into the wall-liquid interface but are computationally expensive, especially for micron-size systems. To this end, coarse-grained particle methods [e.g., lattice-Boltzmann method, smooth particle hydrodynamics, dissipative particle dynamics (DPD)] have been developed in the last two decades to bridge the gap between the atomistic scales and the continuum. These more efficient methods aim to retain important features of the microscopic structure but they may also introduce numerical artifacts through the coarse-graining procedure.

DPD is a relatively new mesoscopic method [2] that describes *clusters* of molecules moving together in a Lagrangian fashion subject to soft quadratic potentials. While DPD has been successfully applied in several simulations of complex fluids [3–5], there are still many unresolved issues that prevent this computationally efficient method from widespread use: they include thermodynamic consistency, coarse-graining artifacts, and anomalous behavior in confined geometries. In this Letter, we report on the last two issues with emphasis on density fluctuations induced by the presence of solid walls. These fluctuations may be physical and thus desirable but in other applications may be erroneous; for example, in colloidal suspensions the artificial layering of a DPD fluid close to the wall may cause spurious depletion forces between the colloids. Unlike the MD method, the soft repulsion between DPD particles cannot prevent fluid particles from penetrating solid boundaries, and thus extra effort is required to impose accurately the no-slip wall boundary condition. This issue of imposing *correctly* the no-slip boundary condition seems to be the main cause of the artificial density fluctuations. There have been several attempts to impose the no-slip boundary condition correctly in DPD simulations of wall-bounded flows [6–9]. They are based on higher density of wall particles, increased values of the repulsive force or reflection of particles near the wall. However, these approaches suffer from either depletion of particles near the wall or artificial ordering of the near-wall particles leading to unacceptable density fluctuations. Some of the proposed methods work well when the conservative force coefficient is zero, however density fluctuations are observed for nonzero values and they increase as these values increase. We note here that similar issues are present in other coarse-grained particle methods, e.g., in smooth particle hydrodynamics, and have been addressed in a series of papers [10–12] resolving most open issues at least for planar geometries, although treatment of complex geometries remains a challenge [12].

As a particle-based mesoscopic method, DPD considers N particles, each having mass m_i, whose momenta and position vectors are governed by Newton's equations of motion. For a typical particle i: $\vec{v}_i = \frac{d\vec{r}_i}{dt}$, $\vec{F}_i = m_i \frac{d\vec{v}_i}{dt}$ where $\vec{v}_i$ its velocity, $\vec{r}_i$ its position, and $\vec{F}_i$ its net force. The interparticle force $\vec{F}_{ij}$ exerted on particle i by particle j is composed of conservative ($\vec{F}^C_{ij}$), dissipative ($\vec{F}^D_{ij}$), and random ($\vec{F}^R_{ij}$) components. Hence, the total force on particle i is given by $\vec{F}_i = \Sigma_{i \neq j} \vec{F}^C_{ij} + \vec{F}^D_{ij} + \Delta t^{-1/2} \vec{F}^R_{ij}$, Δt being the simulation time step. The sum acts over all particles within a cutoff radius r_c beyond which the forces are considered negligible. We set the interaction radius to $r_c = 1$, thus defining the length scale of the system. Denoting $\vec{r}_{ij} = \vec{r}_i - \vec{r}_j$, $\vec{v}_{ij} = \vec{v}_i - \vec{v}_j$, $r_{ij} = |\vec{r}_{ij}|$, and the unit vector $\vec{e}_{ij} = \frac{\vec{r}_{ij}}{r_{ij}}$, the forces are

$$\vec{F}^{\,C}_{ij} = F^{(C)}(r_{ij}) \vec{e}_{ij}, \tag{1}$$

$$\vec{F}^{\,D}_{ij} = -\gamma \omega^D(r_{ij})(\vec{v}_{ij} \cdot \vec{e}_{ij}) \vec{e}_{ij}, \tag{2}$$

$$\vec{F}_{ij}^{R} = \sigma_R \omega^R(r_{ij}) \xi_{ij} \vec{e}_{ij}, \tag{3}$$

where the ξ_{ij} are symmetric Gaussian random variables with zero mean and unit variance and σ_R, γ are coupled by $\sigma_R^2 = 2\gamma k_B T$, k_B being the Boltzmann constant and T the temperature of the system [13]. A common choice for the conservative force is a soft repulsion given by $F^{(C)}(r_{ij}) = a_{ij} \max\{1 - \frac{r_{ij}}{r_c}, 0\}$. The dissipative and random forces, on the other hand, are characterized by strengths $\omega^D(r_{ij})$ and $\omega^R(r_{ij})$ coupled by $\omega^D(r_{ij}) = [\omega^R(r_{ij})]^2 = [\max\{(1 - \frac{r_{ij}}{r_c}), 0\}]^2$. The above relation is necessary for thermodynamic equilibrium [13].

The conservative forces present in the DPD equations can be tailored to describe a variety of interactions $F^{(C)}(r_{ij}) = \nabla V(r_{ij})$, for a potential V. They are also associated with the equation of state of the DPD fluid (see Ref. [14]) since the magnitude $a = a_{ij}$ of the conservative force is determined by the dimensionless compressibility κ^{-1}, i.e.,

$$a = k_B T \frac{\kappa^{-1} N_m - 1}{2\alpha \rho_{\mathrm{DPD}}}, \tag{4}$$

where $\alpha = 0.101 \pm 0.001$. The coarse-graining parameter N_m is defined so that the mass of a DPD particle is N_m times the mass of a single molecule,

$$N_m = \frac{M}{m}. \tag{5}$$

Modifications in the conservative force can be made in order to model the repulsive interaction between wall particles and DPD particles. This can be implemented by employing layers of frozen DPD particles at the wall in combination with bounce-back reflections. The conservative force coefficient of the fluid-solid interactions is adjusted to achieve no-slip conditions at the wall and desired density level in the bulk of the flow [15].

A typical density profile for a Lennard-Jones fluid with $\kappa^{-1} = 15.36$ is shown in Fig. 1. We simulate Poiseuille flow and details of the DPD and corresponding MD simulations can be found in Ref. [16]. The density fluctuations for MD and DPD corresponding to $N_m = 1$ are similar, with the main difference being the large values of the DPD density at the wall. As N_m increases, the density fluctuations in the DPD simulations also increase, with the $N_m = 5$ case exhibiting very large values at the wall and also inside the flow domain. This is not a desired effect, because we expect the fluctuations to decrease as we approach the continuum, i.e., $N_m \to \infty$.

We note that the no-slip boundary condition in Poiseuille flow can be accurately implemented by numerical periodicity, thus avoiding the explicit modeling of wall-particle and DPD-particle interaction. This was demonstrated recently in Ref. [17], where it was proposed to simulate two counter-flowing Poiseuille flows using periodic boundary conditions. Specifically, a rectangular domain is doubled in size in the cross-flow direction with the flow driven by applying a body force to each particle. The direction of the force is opposite in the two halves of the domain. This periodic Poiseuille flow method (PPFM) produces a flow with uniform averaged density profile. The absence of density artifacts make this method useful for studying the bulk Poiseuille flow (in the continuum limit), i.e., without any density oscillations associated with the presence of solid boundaries. While PPFM effectively eliminates density artifacts, it does not model any specific wall structure and cannot be applied in general nonperiodic flow systems. We present next a new model that implements the no-slip boundary condition while at the same time can target a prescribed density profile, i.e., flat or oscillatory.

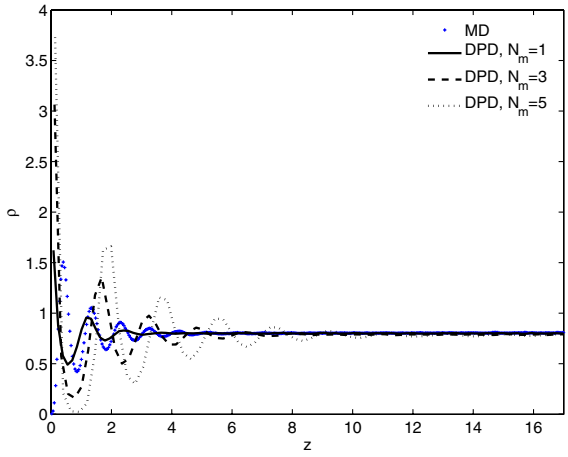

FIG. 1 (color online). Density profiles for Poiseuille flow. The domain extends from one wall to the center line of the channel.

Let us consider a wall perpendicular to the z axis and located at $z = 0$. The wall is moving with the velocity $\vec{V}_W$ remaining in $z = 0$ plane. On each particle within specified distance from the wall we apply a force $\vec{F}^W$ directed perpendicular to the wall, positive in the direction pointing normal into the fluid region. The magnitude of the force $\vec{F}^W$ depends on the distance from the wall and is *iteratively* recomputed based on the estimated density fluctuations as described next. We consider a subregion of the computational domain of width L adjacent to the wall and divide it into bins of size h (see Fig. 2). In general, L should be greater than or equal to the cutoff radius r_c. The value of h can be chosen based on the desired resolution of the simulation results. The total number of bins is then $N_b = L/h$, and we number them in increasing order away from the wall, so that the bin adjacent to the wall has index $i_b = 1$, and the furthest bin from the wall has index N_b. During the simulations in each bin i_b the time-averaged density $\rho_s(i_b)$ is collected over a specified number of time steps N_{av}. Next, the values of ρ_s are *locally* averaged over (up to) n_{av} bins and compared to desired density values ρ_d averaged over the same bins. Specifically, for the bin i_b the densities are averaged over the bins with indices from $i_a = \max(i_b - n_{\mathrm{av}} + 1, 1)$ to i_b. The values of i_a for different bin indices for specific value of $n_{\mathrm{av}} = 3$ used later in this

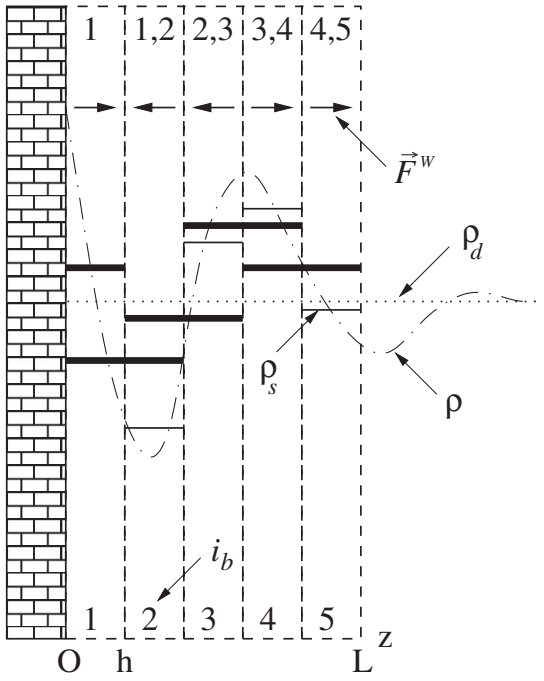

FIG. 2. Sketch illustrating the concept of adaptive boundary condition. The sketch corresponds to the case with parameters $n_{\mathrm{av}} = 2$ and $N_b = 5$ (defined in the text). The bins are shown with dashed lines. The bin indices i_b are shown in a lower part of the bins. The desired (uniform in this case) density level ρ_d is shown with a dotted line. The DPD density profile ρ is shown with a dash-dotted line. The time-averaged density levels ρ_s in the bins are shown with thin solid lines. The locally averaged density levels are shown with thick solid lines. The densities are averaged over the bins with indices from $i_a = \max(i_b - n_{\mathrm{av}} + 1, 1)$ to i_b. These indices are listed in the upper part of the bins. If locally averaged density is higher than desired density the force from the wall $\vec{F}^W(i_b)$ is increased (shown with the arrow pointing away from the wall). If the averaged density is lower, the force is decreased (shown with the arrow pointing toward the wall).

Letter are (i_b, i_a): (1,1), (2,1), (3,1), (4,2), (5,3), etc. The case with $n_{\mathrm{av}} = 2$ is illustrated in Fig. 2. The force $\vec{F}^W(i_b)$ acting on the particles in bin i_b is then updated according to

$$\vec{F}^{\,W}(i_b) = \vec{F}^W(i_b) + C_W\left(\frac{\sum_{i=i_a}^{i_b}\rho_s(i)}{\sum_{i=i_a}^{i_b}\rho_d(i)} - 1\right), \qquad (6)$$

where C_W is a positive constant of order one. After the force is updated, new values of ρ_s are computed and the iterative process continues. The wall force $\vec{F}^W$ is added to the particles within distance L from the wall at each time-integration step. The random and dissipative force contributions from the wall are computed as in Refs. [9,18]. In addition, when fluid particles penetrate into the wall region we perform a ''bounce-back'' reflection of these particles, i.e., we move them back into the fluid region. Typically, we start the simulations with the wall force $\vec{F}^W = 0$ in all bins. We let the DPD fluid equilibrate for a short time (about 1000 steps). As a result large density fluctuations form next to the wall. Next, we apply the adaptive procedure described above. Once the desired density fluctuations are obtained, we collect statistical data from the simulations. We refer to this procedure as adaptive boundary conditions (ABC's).

To evaluate the performance of the proposed model, we have simulated Poiseuille flow using both the periodic (PPFM) and adaptive (ABC) techniques at different levels of coarse graining $N_m \leq 5$. The fluid we consider is governed by a modified Lennard-Jones potential with density $\rho_{\mathrm{MD}} = 0.8\sigma^{-3}$ and occupies a volume of $34.2\sigma \times 8.55\sigma \times 34.2\sigma$; here σ is the atomic diameter in MD. The dimensionless compressibility of the fluid is $\kappa^{-1} = 15.36$ [16]. In DPD units, we have that the length scale is

$$r_c = \left(\frac{N_m \rho^*_{\mathrm{DPD}}}{\rho_{\mathrm{MD}}}\right)^{1/3}\sigma, \qquad (7)$$

where the variables marked with the asterisk have the same numerical values as in DPD but in MD units. The DPD fluid density ρ_{DPD} is chosen to be $3r_c^{-3}$. The time scale is determined by setting the shear viscosities of the DPD and MD fluids equal, thus

$$\tau_{\mathrm{DPD}} = \frac{\nu^*_{\mathrm{DPD}}}{\nu_{\mathrm{MD}}}\left(\frac{r_c}{\sigma}\right)^2\tau. \qquad (8)$$

The viscosity of DPD fluid for each value of N_m can be computed using the Lees-Edwards method [19]. The values of the dynamic viscosity μ for different levels of coarse graining are (N_m, μ): (1,1.04),; (2,1.31), (3,1.55), (4,1.82), (5,2.15). The random ($\sigma_R = 3$) and dissipative ($\gamma = 45$) force coefficients are used in the DPD integration scheme (a modified velocity Verlet method with $\lambda = 0.5$, [14]), time step $\Delta t = 0.02$ and temperature $k_B T = 0.1$, all in DPD units. The DPD simulation parameters can be obtained using Eqs. (4), (5), (7), and (8). All plots, except for the temperature which is normalized by the equilibrium temperature $k_B T = 0.1$, are in reduced MD units.

In the PPFM simulations the domain was doubled in the z direction and the body force $F = 0.0085$ was applied in the x direction. The simulations were run for 410 000 time steps and the domain was subdivided in the z direction into equal bins of size $0.2r_c$, with the data collected over the last 40 000 steps. The simulation results for $N_m = 5$ are plotted in Fig. 3. The DPD density, x velocity, shear stress, and partial temperatures averaged over both halves of the computational domain are shown. The agreement with incompressible Navier-Stokes solution for Poiseuille flow is good for $N_m \leq 5$. For larger values of N_m we observed deviations and above $N_m = 20$ an apparent solidification process is in place; we are currently investigating such effects systematically [18].

In the ABC simulations we integrated the DPD equations for 1 000 000 time steps and the statistical data were averaged over the last 40 000 time steps. A uniform density profile ρ_d was imposed at $\rho_{\mathrm{DPD}} = 3r_c^{-3}$. Also, we used $L = 1r_c$, $h = 0.2r_c$, $n_{\mathrm{av}} = 3$, and $C_W = 1$; the local density values were averaged over $N_{\mathrm{av}} = 500$ time steps.

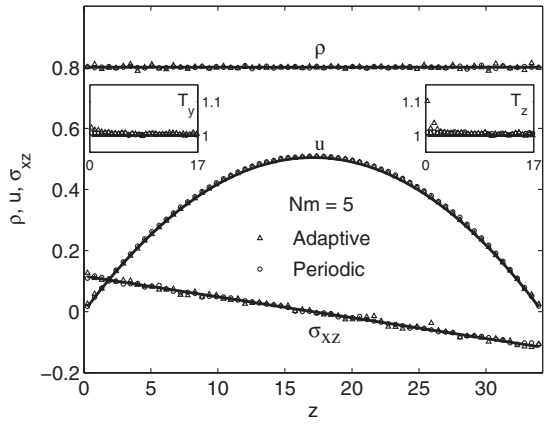

FIG. 3. Comparison of density, velocity, temperature, and stress profiles for Poiseuille flow corresponding to adaptive and periodic boundary conditions ($N_m = 5$). The incompressible Navier-Stokes solution is shown with lines.

Typically, about 50 wall force adjustments in simulations were enough to obtain desired density values close to the wall. The simulation results are shown in Fig. 3 for $N_m = 5$; for $N_m < 5$ similar results were obtained. In general, they are in a good agreement with those obtained from the PPFM method, although there is a difference in the temperature profile close to the wall.

The reason for an increase of partial temperature in the normal to the wall direction is the wall force $\vec{F}^W$. In simulations presented here, an average increase of partial temperature in the z direction was about 11% while the total temperature increase was about 4%. It is possible to affect the temperature close to the wall by modifying the dissipative force coefficient γ of DPD particles. The procedure we apply for adjusting the temperature is similar to one used for the density. Specifically, the coeffcient γ of particles in the bin close to the wall is increased if the temperature is above the desired level in that bin or decreased otherwise. This can effectively control the total temperature; however, the difference between the partial temperatures in normal and parallel to the wall directions remains about the same. For example, for the case considered here with $N_m = 5$ the average increase of partial temperature dropped by 3–4% and the total temperature was within 2% of $k_B T = 0.1$.

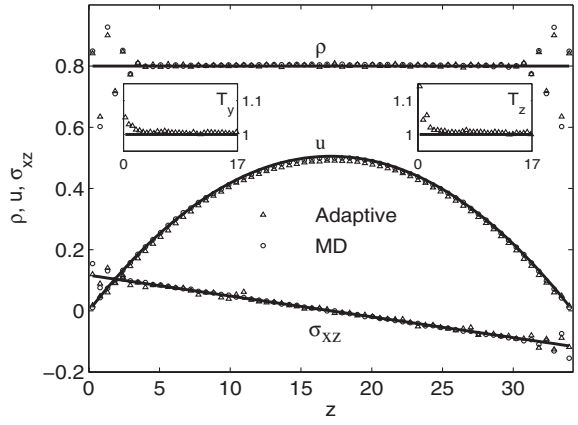

FIG. 4. Comparison of density, velocity, temperature, and stress profiles for Poiseuille flow corresponding to adaptive boundary conditions and coarse-grained MD results ($N_m = 5$).

Finally, we demonstrate that the ABC approach can be employed to target specific density fluctuations close to the solid wall. Here, for illustration purposes, we present a case, where the density fluctuations imposed by boundary conditions in DPD correspond to the coarse-grained MD density fluctuations. Specifically, the coarse-grained density fluctuations close to the wall are obtained from MD simulations by averaging them in bins of size $0.2r_c$, where the value of DPD unit of length r_c corresponds to $N_m = 5$; see Eq. (7). The fluctuations are significant within distance of $2r_c$ from the wall and therefore we chose $L = 2r_c$ in the ABC method. In addition, we set $h = 0.2r_c$, $N_{\text{av}} = 500$, $n_{\text{av}} = 3$, and $C_W = 1$. The desired level for density fluctuations ρ_d in each bin is set based on coarse-grained MD data. In Fig. 4 we plot the MD and DPD simulation results. In general, the density, velocity and stress profiles are in good agreement, although the DPD temperature is increased close to the wall due the aforementioned reasons.

This work was supported by the NSF-IMAG program.

*Electronic address: piv@dam.brown.edu
†Electronic address: gk@dam.brown.edu

[1] G. E. Karniadakis, A. Beskok, and N. Aluru *Microflows and Nanoflows: Fundamentals and Simulation* (Springer, New York, 2005), 2nd ed..
[2] P. J. Hoogerbrugge and J. M. Koelman, Europhys. Lett. **19**, 155 (1992).
[3] N. A. Spenley, Europhys. Lett. **49**, 534 (2000).
[4] R. D. Groot and K. L. Rabone, Biophys. J. **81**, 725 (2001).
[5] A. Maiti and S. McGrother, J. Chem. Phys. **120**, 1594 (2004).
[6] Y. Kong, C. W. Manke, W. G. Madden, and A. G. Schlijper, Int. J. Thermophys. **15**, 1093 (1994).
[7] J. L. Jones, M. Lal, J. N. Ruddock, and N. A. Spenley, Faraday Discuss. **112**, 129 (1999).
[8] M. Revenga, I. Zuniga, P. Espanol, and I. Pagonabarraga, Int. J. Mod. Phys. C **9**, 1319 (1998).
[9] S. M. Willemsen *et al.*, Int. J. Mod. Phys. C **11**, 881 (2000).
[10] H. Takeda, S. Miyama, and M. Sekiya, Prog. Theor. Phys. **92**, 939 (1994).
[11] L. Sigalotti, J. Klapp, E. Sira, Y. Melean, and A. Hasmy, J. Comput. Phys. **191**, 622 (2003).
[12] R. Ata and A. Soulaimani, Int. J. Numer. Methods Fluids **47**, 139 (2005).
[13] P. Espanol and P. Warren, Europhys. Lett. **30**, 191 (1995).
[14] R. D. Groot and P. B. Warren, J. Chem. Phys. **107**, 4423 (1997).
[15] I. V. Pivkin and G. E. Karniadakis, J. Comput. Phys. **207**, 114 (2005).
[16] E. E. Keaveny *et al.*, J. Chem. Phys. **123**, 104107 (2005).
[17] J. A. Backer *et al.*, J. Chem. Phys. **122**, 154503 (2005).
[18] I. V. Pivkin, Ph. D. thesis, Brown University, 2006.
[19] A. W. Lees and S. F. Edwards, J. Phys. C **5**, 1921 (1972).